Chitosan modified N, S−doped TiO_2 and N, S−doped ZnO for visible light photocatalytic degradation of tetracycline

Negin Farhadian[a], Rokhsareh Akbarzadeh[b], Meghdad Pirsaheb[a], Tien-Chien Jen, Anvar Asadi[a*]

[a]Research Center for Environmental Determinants of Health, Kermanshah University of Medical Sciences, Kermanshah, Iran

[b]Mechanical Engineering Department, Faculty of Engineering and the Built Environment, University of Johannesburg, 2006, South Africa (rakbarzadeh@uj.ac.za)

ABSTRACT

N, S− doped TiO_2 (NST), N, S− doped ZnO (NSZ) and their composite with chitosan (NST/CS, NSZ/CS) were synthesized by sol gel-hydrothermal method. Chitosan modified and unmodified NST and NSZ were characterized using XRD, FTIR, TEM and BET techniques. These photocatalysts were used for the photocatalytic degradation of tetracycline under visible light irradiation. Based on screening test, NST/CS had the highest tetracycline degradation efficiency of 91% for the short duration of 50 min under visible light irradiation. The blending of chitosan with NST increases the rate of photocatalytic degradation of tetracycline about 2 times. A detail characterization including HRTEM, SEM, EDS and DRS were conducted for NST/CS, the most active photocatalyst. Photocatalytic activity test was conducted by varying tetracycline concentration, irradiation time, catalyst's concentration and pH using response surface methodology (RSM) based on central composite design to find out the optimum condition for photocatalytic activity. The reusability of as-synthesized NST/CS was assessed and due to high recoverability can be applied as an effective catalyst for degradation organic substances in water and wastewater especially for degradation of emerging pollutants such pharmaceutical pollutants. The results from this work show a

*Corresponding author. Email Addresses: Anvarasadi@sbmu.ac.ir, (A. Asadi)

promising technology for local authorities and pharmaceutical facilities to remove tetracycline in water resource.

Keywords: Chitosan; Nitrogen and sulfur co-doped TiO_2; Nitrogen and sulfur co-doped ZnO; photocatalysts; Tetracycline

1. Introduction

Pharmaceutical antibiotics are emerging pollutants of particular concern because of their widespread use in human therapy and the farming industry (Gao et al., 2012). In 2010 the usage of antibiotics more than 70 billion standard units (i.e. tablets) in human consumption was reported and their use in livestock production exceeded 63000 tones (Norvill et al., 2017). The most of antibiotics are incompletely absorbed by organisms in human and veterinary medicine (60-90% of antibiotics dose are discharged through urine and feces). Therefore, they are present in soil, agricultural runoff, effluent of wastewater treatment plants, groundwater, and even in drinking water (Shao et al., 2012). On the other hand, only 60–90% of antibiotics could be removed by conventional treatments such as flocculation and biological treatment (Kakavandi et al., 2016). Moreover, continuous release of antibiotics such as tetracycline (TC) into water is a serious threat to human health through creation of antibiotic-resistance bacteria (Nasseh et al., 2018). These bacteria can be transferred and spread antibiotic resistant genes among microorganisms which can disrupt indigenous microbial populations (Acosta et al., 2016; Ahmed, 2017; Gao et al., 2012). Therefore, the presence of antibiotics including TC from water is a public health concern and their removal is a challenge for scientific community.

Large molecules of TC are quite hydrophilic with solubility which is in the ranges of g/L which lead to lower sorption on adsorbent like activated carbon (Chang et al., 2009). Recently, advanced oxidation processes (AOPs) utilizing heterogeneous photocatalysis using photocatalysts such as zinc oxide (ZnO) and titanium dioxide (TiO_2) has attracted much attention for degradation of hazardous organic compounds (Ani et al., 2018; Bahrami et al., 2018). These photocatalysts generate a powerful oxidant, hydroxyl radical

(•OH), which can promote the degradation process (Karthikeyan, K.T. et al., 2017; Pirsaheb et al., 2018). Among various semiconductors employed, TiO_2 and ZnO are among the most preferable photocatalysts due to their non-toxic, simple synthesis, insolubility, stability, outstanding optical and physical properties, high photoactivity and low cost (Bozorgpour et al., 2016; Zainal et al., 2009). However, these semiconductors are only activate under ultraviolet (UV) light of wavelengths $\lambda \leq 390$ nm, and this limits the use of theses photocatalyst under sunlight (about 4% of the solar spectrum is UV). These semiconductors also have high electron-hole recombination rate which limit their practical applications (Zhu et al., 2012). There are a lot of researches on modification of TiO_2 and ZnO, e.g. deposition of noble metals, coupling of semiconductor, dye sensitizing doping with metals (Ag, Pt, Au, Mg) and non-metals doping (i.e. N, S, C, P, F) to enhance the photocatalytic performance of semiconductors under the visible light and also to control the recombination rate (Eslami et al., 2016). For example, Qiu and co-workers (Qiu et al., 2013) synthesized nitrogen doped ZnO for photocatalytic degradation of bisphenol A under the visible light. They observed that N doped ZnO, under visible light, could degrade 93% of BPA which was much higher than the rate in pure ZnO and Degussa TiO_2 P25. However, practical application of TiO_2 and ZnO nanoparticles is still facing limitations such as the reusing of photocatalysts. Moreover, great tendency of TiO_2 and ZnO nanoparticles to aggregate which increases at high concentrations is another constrain (Nawi et al., 2011). An alternative convenient method to solve this problem is to immobilize these semiconductors on solid supports which after reaction facilitate the separation and recycling of the photocatalysts. These supporting materials should have properties such as controllable pore space and surface chemistry, easy recovery, good mechanical strength for long-term use.

In recent years, various biopolymers, clays, grapheme and cellulose have been used to enhance the mechanical stability and the efficacy of the photocatalytic materials. Among them, chitosan (CS) is a very important biopolymer, which is not only abundant, but also provide high adsorption potential for a broad range of organic compounds, pesticides, and heavy metal ions, and is biocompatible (Bozorgpour et al., 2016; Zainal et al., 2009). CS is a natural biopolymer derived by partial N-deacetylation of chitin (a linear

polymer of N-acetyl-2-amino-2-deoxy-d-glucopyranose units with ß–(1–4) bonds) and is a main component of crustacean shells such as crab, shrimp, and craw fish (Karthikeyan, K.T. et al., 2017). Therefore, nano-composites of chitosan, derivatives from chitosan and modified oxides would be applied in more wide fields with multi-functionalities (Kannusamy and Sivalingam, 2013; Zhang et al., 2015). Accordingly, Karthikeyan et al (Karthikeyan, K. et al., 2017) reported the photocatalytic and antimicrobial activities of chitosan-TiO_2 nanocomposite and it was effective against both Gram-positive and Gram-negative bacteria and a zone of inhibition ranged between 10.333 ± 0.5773 and 25.667 ± 1.5275 (mm) was observed. In another study Dhanya and Aparna (Dhanya and Aparna, 2016) synthesized TiO_2/Chitosan based hydrogel and removed almost entirely Azo and Anthraquinone dyes from wastewater. Hence in the present study, modified TiO_2 and ZnO powders were introduced into the chitosan matrix to form a nanocomposite using sodium tripolyphosphate (STPP) as a cross-linker.

Based on the above facts about TiO_2, ZnO and chitosan, we used thiourea as precursor of nitrogen and sulfur for synthesizing of NST and NSZ through simple mixing-calcination method. Then, NST/crosslinked chitosan composite (NST/CS) and NSZ/crosslinked chitosan composite (NSZ/CS) were successfully synthesized. These photocatalysts were used to photocatalyze TC (as a model pollutant) under visible light irradiation (fluorescent lamp). The morphological and physicochemical characteristics of the synthesized catalysts well characterized using different experimental techniques including: Fourier transform infrared spectroscopy (FTIR), X-ray diffraction (XRD), transmission electron microscope (TEM) and N_2 adsorption–desorption isotherms. Moreover, after determining the optimum catalyst, its characteristics was further evaluated using high resolution transmission electron microscope (HRTEM), scanning electron microscopy with energy dispersive X-Ray spectroscopy (SEM-EDS) and diffuse reflectance spectroscopy (DRS). After selecting best catalyst through screening test, the effects of catalyst dose, pH, TC concentration and irradiation time were examined. Moreover, the reusability and effect of real wastewater matrix for the best catalyst was preliminarily evaluated. These results will be helpful for further application of most active photocatalysts for the effective degradation of pharmaceutical containing effluents.

2. Materials and methods

2.1 Raw materials

Acetic acid, thiourea, chitosan (medium molecular weight), sodium hydroxide, sodium tripolyphosphate (STPP), hydrochloric acid were purchased from Merck and used as received. ZnO and TiO_2 P25 Degussa nanoparticles were purchased from Nanoespadena, Iran and Degussa Corporation, Germany, respectively.

2.2 N,S co-doped TiO_2 (NST) and N,S co-doped ZnO (NSZ) preparation

At first, 2 grams of thiourea and 1 grams of Degussa TiO_2 P-25 in a 2:1 (w/w) ratio were placed inside an agate mortar and crushed/rubbed for one hour to completely mix together. The calcination of catalyst powder was performed at 400 °C for 2 hours under air atmosphere in a furnace with a heating rate of 10 °C per minute. Then mixture was allowed to cool down at ambient temperature inside a desiccator, thereafter it was washed 3 times with distilled water, dried at 70 °C and crushed to form a fine NST powder. The preparation of the NSZ was similar to TiO_2 nanoparticle, with the difference that the calcination was carried out at 600 °C for 6 hours.

2.3 Preparation of N,S co-doped TiO_2 /chitosan (NST/CS) and N,S co-doped ZnO/chitosan (NSZCS)

NST/CS and NSZ/CS nano-composites were prepared using NaOH as oxidizing agent and sodium tripolyphosphate (STPP) as the cross-linking agent. In summary, 1 g of chitosan and 0.5 g of NST and NSZ catalysts were separately dissolved in 35 ml of distilled water. To each solution 2.5 ml of acetic acid was added and stirred vigorously to obtain a clear viscous solution. After dissolution of chitosan in acid, the pH was adjusted to the highest possible level (about 6.5) by using sodium hydroxide, which helps to have the lowest free proton in the environment. Then, the homogeneous viscose solution then through a syringe dropwise was added to 400 ml of aqueous solution containing 4 g STPP and 3.2 g NaOH. The viscose solution was added to STPP/NaOH solution which formed the beads, this was kept for 24 h to crosslink with STPP. After 24 hours, the solution was filtered and the precipitant was washed several times with

distilled water and was dried at 80 ° C for 24 hours. The dried photocatalyst was ground to fine powder and used for photocatalytic degradation study.

2.4 Catalyst characterization

X-ray powder diffraction (XRD) of prepared photocatalysts were analyzed by a Bruker AXS D8 Advance instrument (USA). The patterns with a Cu Kα (λ=1.5406 Å) radiation were taken over the diffraction angle (2θ) range of 10-90°. The Scherrer's equation (Langford and Wilson, 1978) was used to estimate average crystalite size of particles. Morphological features and surface characteristics of the synthesized photocatalysts were obtained by SEM using a Hitachi SX-650 scanning electron microscope. The transmission electron microscopy (TEM) and high resolution electron microscopy (HRTEM) investigation were carried out using JOEL JEM-2100 electron microscope (Japan). Nitrogen adsorption/desorption isotherms were measured by a Belsorp mini II (Japan) at 77.35 K. Specific surface area (SSA) and textural properties of pores such as their size, volume and distribution were calculated using BET and BJH isotherm models. FTIR spectra of photocatalysts were recorded in the region of 400-4000 cm^{-1} at room temperature using a Fourier-Transform IR spectrometer (WQF-510A/520A). DRS of the NST/CS nano-composite was done by an Avantes spectrophotometer (Avaspec-2048-TEC) with a $BaSO_4$ as a reference material.

2.6 Photocatalytic experiments

Photocatalytic degradation experiments were conducted in a batch reactor and at room temperature. To prepare different concentrations of the TC, its stock solution was dissolved in distilled water. Initially , the pH of the TC solution was adjusted by NaOH and HCl solutions. The reactor was placed on a magnetic stirrer. Both the reactor and stirrer were placed in a photocatalytic chamber containing 6 LED lamps (18 W). Firstly, 100 mL of TC solution (25mg/L) were taken and the pH was adjusted to 7. To find out the photolysis percentage the experiment was conducted without photocatalyst. The effect of TC adsorption on photocatalysts was examined in absence of light irradiation under identical conditions. Therefore, the same volume of solution was mixed with photocatalyst and prior to photocatalytic experiments, the solution

mixture left on a magnetic stirrer in the dark condition to reach the adsorption-desorption equilibrium. Subsequently the photocatalytic experiment was continued under the visible light irradiation. This steps were repeated for all the samples to find out the best photocatalyst. After screening of of the best photocatlyst, the effect of pH (5-9), photocatalyst dose (0.5-2.5 g/l), TC concentration (10- 50 mg/l) and time (20-60 min) were studied based on the design of experiments method. Finally, reusability tests were carried out at optimal operating conditions determined under response surface methodology. Samples were taken at specified time intervals, and 0.22 μm filter was used for the photocatalyst particles removal. The concentration of TC was measured using UV spectroscopy (Agilent 8453, USA) at 360 nm. The adsorption, photolysis and the percentage of ptotocatalytic degradation efficiency (R for removal??) of TC were calculated using following equation:

$$R(\%) = \frac{(C_0 - C_e)}{C_0} \times 100 \qquad (1)$$

Where C_0 and C_e (mg/L) are the initial and final concentration of TC, respectively.

2.7 Experimental design and procedure

After finding the best photocatalyst at default experimental conditions, response surface methodology (RSM) model based on central composite design (CCD) was used to design the experiments for finding the mutual effects of the influencing experimental variables and to optimize TC degradation by NST/CS under visible light irradiation. The influence of operating factors such as pH of solution, photocatalyst dosage, reaction time and initial concentration of TC on the performance of system were studied in a batch mode. The five various levels of selected independent parameters are displayed in Table 1.

Table 1

3. Results and discussion

3.1. Characterization of catalysts

3.1.1. X-ray diffraction (XRD)

The XRD pattern of the pure TiO_2 (Degussa P25), pure ZnO, NST, NSZ, NST/CS and NSZ/CS is shown in Fig. 1. The pure TiO_2 and pure ZnO were only used as references for the comparison (blank sample). For TiO_2 samples, both anatase and rutile phases were observed with fraction content of 82% and 18%, respectively which matches with the JCPDS card no. 21-1272 (anatase) and no. 21-1276 (rutile). However, the mix-crystal titania structures has the higher photoactivity than the single anatase or rutile phase (Shao et al., 2008). For the ZnO, XRD pattern can be indexed to wurtzite structure which is well matched with the standard card for the hexagonal ZnO crystal (JCPDS card no. 36-1451) (Rastkari et al., 2017). For both TiO_2 and ZnO samples, nitrogen and sulfur doping didn't cause significant change in crystal structure. This indicates that doping of TiO_2 and ZnO by nitrogen and sulfur have no effect on their crystal structure, which may due to the low percentage of the nitrogen and sulfur below XRD detection limit (Eslami et al., 2016; Qiu et al., 2013). A small and shoulder peak around $2\theta=13°$ and amorphous diffraction peaks at $2\theta=19.9°$ (Fig. 1b) are due to the blending of CS in the nano-composites (NST/CS and NSZ/CS). However, addition of chitosan (CS) doesn't significantly change the crystal structure of TiO_2 and ZnO which may due to its low loading in the composites. The similar results were reported in the previous literature (Kamal et al., 2016; Saravanan et al., 2018). The crystallite size of photocatalysts was estimated using Scherrer equation as follow:

$$D = \frac{K.\lambda}{\beta.\cos(\theta)} \qquad (1)$$

where D is average crystalline size [nm], K is Shape Factor, λ Wavelength of X-rays [nm], β is the full-width half maximum of the diffraction peak [Rad], and θ is Bragg Angle. [°]. Therefore, the crystallite sizes of NST, NST/CS, NSZ and NSZ/CS were calculated to be 18.7, 35.3, 24.3 and 36.2 nm, respectively. The

blending of CS with N,S-TiO_2 and N,S-ZnO samples cause a slight increase of the mean crystallite sizes. However, average particles size of doped and un-doped samples didn't have significant change.

Fig. 1.

3.1.2. TEM, HRTEM and SEM profiles

The morphology of prepared samples was characterized through TEM. As can be seen in figure 2a, TEM images, all photocatalysts particles have tetragonal crystalline structure with mean size between 12 to 50 nm. Moreover, the particle sizes obtained from TEM are comparable to those calculated from Scherrer's equation using XRD data. TEM images also shows that the particles in NST and NST/CS catalysts were clear and well separated although in the NST/CS catalyst some of them partially aggregated. It is noted that the NSZ and NSZ/CS products mainly consist of agglomerated nanoparticles which is more obvious in sample NSZ/CS, which may have occurred due to the occurrence of charging effect.

To further confirm the formation of the NST/CS nano-composite, HRTEM images was obtained. Fig. 2b shows the HRTEM of NST/CS nano-composite (as an optimum catalyst). As shown in Fig. 2b, for NST/CS sample lattice spacing of 0.35 nm, 0.32nm, 0.43 nm and 1.5 nm were measured. The lattice spacing of 0.34 nm corresponds to the (101) plane of the tetragonal anatase phase TiO_2 (JCPDS 21-1272). Lattice spacing of 0.32 nm corresponds to the (110) plane of the rutile phase TiO_2 (JCPDS 21-1276). These spacing are in agreement with the d-spacing obtained by XRD analysis. Lattice spacing of 0.80 nm and 1.5 nm can be referred to the effect of NS and chitosan on lattice spacing of nanoparticles.

Fig. 2.

The SEM image, elemental mapping and EDS spectra for the NST/CS are shown in Fig. 2c and d. The whole surface area of chitosan was covered by TiO_2 particles. Highly-ordered mesoporous TiO_2 nanoparticles were obtained and as a multi layers immobilized on chitosan. EDS confirmed the presence of major elements such as C, O, Ti and P. The large amount of O and C elements are the result of chitosan matrix in NST/CS.

3.1.3. The specific surface area, pore size and pore volume

Figure 3 shows nitrogen adsorption–desorption isotherms as well as pore size distribution curves (inset) of samples. It was observed that all samples have type IV isotherms and very narrow hysteresis loops at relative pressures close to unity which indicate the presence of large well-developed mesoporosity (size between 2 and 50 nm). This phenomenon is more obvious for NSZ and NSZ/CS samples which reflecting high external surface area of the sample which can be due to the presence of macropores (widths> 50 nm). Moreover, Fig. 3 (insect) shows the plots of pore-size distribution which shows NSZ and NSZ/CS samples have broader ranges, and it confirmed the existence of mesopores and macropores. The pore size of NST/CS is broader than NST, indicating that chitosan cause increase in the crystallinity of photocatalysts. However, mesopores and macropores were formed during nanoparticles aggregation because single single-crystal of them is nonporous. Such porous materials are extremely useful in photocatalysis due to their ability to promote the molecular transport of both products and reactants (Xiang et al., 2011; Yu et al., 2010). Table 2 shows the specific surface area (S_{BET}) of photocatalysts which measured by the BET method by N_2 adsorption and desorption at –195.8 °C. The blending of CS with NST and NSZ cause drastic reduction in specific surface area of NST/CS and NSZ/CS nano-composites. The diversity trend of the pore volume is similar to the specific surface area which NSZ have bigger pore volume than the other photocatalysts. The highly decrease in S_{BET} and pore volume of CS blended samples might give an adverse effect on their activity, but NST/CS had the highest photocatalyst activity. However, the activity of a photocatalyst can be only related to the catalyst surface area or not is still an ambiguous issue, because photocatalytic reactions are believed to proceed only on the irradiated surface (Yu et al., 2010). Therefore, the difference in photocatalytic activity between these catalysts, are the result of light absorption which is a key factor in photocatalysis.

Fig. 3.

Table 2

3.1.4. FTIR spectra

FTIR spectra of NST, NST/CS, NSZ, and NSZ/CS photocatalysts are shown in Fig. 4a and b. The FTIR spectra of all samples show similar features except for wavenumbers smaller than 1100 cm-1. The peaks of the FTIR spectra become more intense in the case of chitosan composites (NSZ/CS and NST/CS). Compared with FTIR spectra of NSZ and NST, spectra of NSZ/CS and NST/CS composites indicate new peaks between 400-800 cm^{-1} regions that were attributed to the bands of metal oxide bonds which confirm the formation of Zn-O and Ti-O bonds and hence confirming the existence of chitosan in nano-composite matrix. These metal oxides, ZnO and TiO_2, occur at the fingerprint region of IR at lower wavelength around 520 cm^{-1}, respectively. This indicates the strong interaction between these groups and TiO_2 which could be due to strong attachment of NST to the amide groups. The characteristic absorption bands for chitosan could also observe at wavenumbers below 1070 cm^{-1}. In NSZ/CS sample Band at 1070 assign to C-O-C stretching vibrations (Gregorio-Jauregui et al., 2012). In both NSZ and NSZ/CS samples, the peak at 526 cm^{-1} confirming the formation of ZnO as suggested by Martinez and his colleagues (2011) (Martinez et al., 2011). The FTIR spectra of all samples exhibited a band of multiple peaks, 2900 and 3100 cm^{-1}, which is due to stretching vibration of C-H and N-H groups. The absorption peaks at 1700 cm^{-1}, 1490 $cm^{-1}$and 1400 $cm^{-1}$are ascribed to bending vibration of C=O stretching group, N-H and C-H group in CH_2OH. 1400 cm^{-1} band could also be assigning to asymmetric C-S group of thiourea. FT-IR spectrum of NST and NSZ show peaks at lower wavenumber which belongs to metal oxide bonds stretching vibration. In thiourea there is usually a broad and intense peak between 3000 and 4000 cm^{-1} for NH_2 which can't be seen in these spectra. Similarly, there is usually a broad and intense peak due to presence of chitosan which should appear between 3000 and 4000 cm^{-1} for OH functional group which was not detected in this study most probably due to the calcination process.

Fig. 4.

3.1.5. UV–visible diffuse reflectance spectroscopy (DRS)

Figure 5 shows the UV–visible absorption spectra of NST/CS photocatalyst as an efficient catalyst for degradation of TC. Diffuse reflectance spectra of NST/CS showed an absorption tail in the 400–800 nm region due to the presence of N and S co-doping and CS blending which shift the wavelength response range into the visible region. The enhanced absorbance around 500 nm related to nitrogen doping and around 630 nm is possibly due to the synergistic coexistence of nitrogen and sulfur on TiO_2 electronic structure. The inset in Fig. 5 shows the plot of $(F(R_\infty)*h\nu)^{0.5}$ versus hν (eV) which allows to evaluate the band gap energy (Salarian et al., 2016). It turns out that NST/CS has band gap energy of 2.6 eV, calculated term of absorption coefficients $F(R_\infty)$ by the transformed Kubelka–Munk ($F(R_\infty) =(1- R_\infty)/2\ R_\infty$) function. The NST/CS lower band gap is probably due to co-doping of N,S and subsequently formation of an intra-gap states above the valence band, oxide centers substitution by sulfur/nitride centers and/or the interstitial addition of sulfur/nitride to the oxide lattice (D'Arienzo et al., 2009).

Fig. 5.

3.2. Photocatalytic experiments

3.2.1. Photolysis and dark adsorption capability of catalysts

A photolysis test is necessary to determine the contribution of the photolysis alone in the heterogeneous photocatalytic processes, because if a selected model organic compond has a high degradation rate via only photolysis, it is not necessary to carry out the design of catalytic systems to eliminate it. Therefore, the photolysis of TC under irradiation alone at defined operating conditions (pH 7 and 25 mg/l of TC) was investigated at 60 min and the results are shown in the Fig. 6. According to the Fig. 6, the photolysis in the absence of photocatalyst could contribute 25% of TC removal in 60 minutes.

Fig. 6.

To determine the adsorption capacity of the photocatalyst, the adsorption test was conducted. A dark adsorption experiment was carried out at pH of 7, photocatalyst dose of 1 g/l, TC with concentration of 25 mg/l and time duration of 60 min. Figure 7 shows the changes of the TC adsorption onto NSZ, NSZ/CS, NST and NST/CS for the duration of 60 min. For all adsorbents, the adsorption rate was very high in the

first 30 minutes, and after that, almost all catalysts had reached the equilibrium state. The rapid absorption of the drug in the first 30 minutes reflects the physical absorption process. The NSZ catalyst has the highest adsorbance of approximately 80% in the first 30 minutes, and the NST/CS catalyst with 25% has the lowest adsorption potential against tetracycline. The higher adsorption efficiency of NSZ than other catalysts is attributed to its large porosity (0.36 cm^3/g) and high surface area (17.80 m^2/g). In contrast, the NST/CS catalyst had the least amount of drug absorption because of its BET surface area (0.49 m^2/g) and pore volume was 0.011 cm^3/g. Moreover, although the amine groups exist on the tetracycline have little ionization ability, but this small amount gives a small amount of local positive charge to the molecule. Due to the fact that chitosan is also positive, it affects the adsorption slightly and thus the lower sorption of TC on the NST/CS composite compared to the NST alone was observed.

Fig. 7.

To determine the optimal photocatalytic system, a set of photocatalytic experiments were conducted under ascribed conditions (pH 7, catalyst dose of 1.0 g/l, drug concentration of 25.0 mg/l and irradiation time of 60 min). Prior to photocatalyst degradation experiments, four prepared systems were placed in the dark for 15 minutes under mechanical stirring conditions to ensure an adsorption/desorption equilibrium. Obtained results are presented in Fig. 8. As it is clear from the Fig. 8, two catalysts, NSZ and NST/CS, exhibit the most photocatalytic elimination during 60 minutes irradiation. According to the results of the absorption test and the high absorption ability of NSZ catalyst at the desired time, NST/CS catalyst was selected as the optimal catalyst system for photocatalytic degradation tests of TC. Considering the low adsorption of the NST/CS catalyst, it can be concluded that the photocatalytic degradation is the main mechanism for TC degradation. Both adsorption/photo-degradation processes are involved in degradation of TC by organic–inorganic NST/CS hybrid catalyst. Adsorption mainly occurred due to inter and intramolecular H-bonds interaction between chitosan functional groups (NH_2 and OH groups) with the polar groups of TC (Chiou et al., 2004; Wu et al., 2001; Zainal et al., 2009). Besides the benefits of chitosan in adsorption of drug

molecules, the excellent photocatalytic performance of the NST/CS composite could be ascribed to the incorporation of N, S to the TiO_2 surface which improve the light absorption in visible region and also photo-induced electron-holes separation and transfer (Cheng et al., 2013). The linear fit between $\ln(C_t/C_0)$ and irradiation time can be used to explain the pseudo-first-order kinetics of synthesized photocatalysts. Results are shown in Fig. 9 inset. As can be seen, the NST/CS catalyst had the highest correlation coefficient and rate constant, 0.95 and 0.048 min^{-1}, respectively.

Fig. 8.

The lower photocatalytic activity of NST compared to its chitosan composite (NST/CS), can be explained by the fact that the binding of the drug to the surface of the nano-composite reduces the optical properties and therefore its catalytic effect while chitosan reduces such a destructive effect. Chitosan improves the photocatalytic performance of nano-composites by preventing the drug from joining the surface of the nanoparticle. But for the NSZ nano-composite, there are different results. In this case, the extraordinary ability of the ZnO to adsorb the drug has greatly affected the results. According to the results of the adsorption test, it can be said that in the case of NSZ/CS a large percentage of the drug in the photocatalytic process is actually not photo-degradaed but adsorbed on the nano-composites.

After defining the photocatalytic system with the highest efficiency in TC degradation, to optimize the NST/CS catalyst performance and determine the main and mutual effects of the influencing operating parameters on the photocatalytic process, design of experiment tools was used.

As shown in Table 3, based on the design matrix, 30 experimental runs were conducted to evaluate the photocatalytic degradation process.

Table 3

According to the obtained results, the quadratic model (Eq. (1)) is presented to predict the results:

$$R(\%) = 57.40 + 2.55A + 3.80B - 2.31C + 6.69D - 6.30AB + 9.32AC - 0.33AD$$
$$+3.67BC + 0.75BD - 0.11CD + 4.71A^2 + 3.44B^2 + 3.31C^2 + 2.06D^2 \quad (1)$$

All considered variables can affect the photocatalytic efficiency in a different way. Equation terms with positive coefficients have direct effect and each term with negative sign have an inverse effect on the process efficiency.

To judge the significance and adequacy of the predicted model, the results of variance analysis (ANOVA) are shown in the Table 4. The degree of importance of the variables considered in the model can be determined by using ANOVA information including P-value, F-value, R^2, and adjusted R^2. A very low P-value of the predicted model demonstrates the high significant of it. According to ANOVA, two main effects (B, D), two interaction effects (AB, AC) and three second order effects (A^2, $B^2$and C^2) have a P-value less than 0.05 and will have a larger contribution in the model predictions. The high values of R^2 and adjusted R^2 close to 1 indicate a good agreement between experimental data and model predictions (Nasseri et al., 2018).

Table 4

It is clear from the normal probability plot of the residuals (Fig. 9a) that the data doesn't have a specific pattern and has been randomly scattered over a straight line and indicate good adequacy of the regression model. Also from the Fig. 9b, the actual data are in close agreement with the predicted ones.

Fig. 9.

To understand and visualize the main effect and interaction effects between variables, response surface plots are applied. For each three dimensional surface plots, the two variables are kept constant in their central value, and the two other variables are changed in their selected ranges. The response surface plot of the TC degradation using NST/CS photocatalyst under visible light irradiation as the function of four variables are shown in Fig. 10a-f. As evident from Fig. 10, by increasing the irradiation time, the TC degradation efficiency was enhanced. Moreover, when the initial concentration of the TC changes from 20 mg/l to 40 mg/l, the degradation efficiency decreased approximately from 76% to 56%. This reduction can be due to saturation of the available active surface sites by more TC molecules and lowering of photons interaction (SİMSEK, 2017). After saturation, the contact of drug molecules with photo-induced holes declined. Also, the increase in initial concentration leads to adsorption of more TC molecules and

occupation of the active sites and subsequently reduction of the hydroxyl radicals formation at the photocatalyst surface (Bechambi et al., 2015; Gu et al., 2010; Nezamzadeh-Ejhieh and Karimi-Shamsabadi, 2013). Generally, different values of pH significantly affected the degradation rate of TC and the higher degradation rate was observed in slightly alkaline condition. The reason for the higher degradation efficiency in weak alkaline conditions (pH 8) can be ascribed to the production of hydroxyl radicals more rapidly in these conditions (Buxton et al., 1988; Hayon et al., 1972). Increasing the NST/CS photocatalyst concentration in the reaction solution caused an increment of the degradation efficiency mainly due to the increase in the available active sites and surface photon absorption.

Fig. 10.

3.2.2. Optimization of operating conditions

Determining the optimal catalyst dose with maximum TC degradation capability is an essential step for designing of an efficient photocatalytic system. In order to determine the optimal operating condition, the goal is to achieve the maximum amount of antibiotic degradation when all the operational variables are located within their experimental ranges. The optimum TC degradation efficiency reached 91% with desirability of 1.0. The numerical optimization which shows four goals of the studied process are presented in Fig. 11.

Fig. 11.

3.3. Reusability of the NST/CS nanocomposite

To determine practical applications of the optimum NST/CS photocatalyst, the stability/recoverability and the reusability of the catalyst for TC degradation was evaluated. In this regard experiment was repeated four times under optimal condition of operating parameters. At the end of each test, photocatalyst was centrifuged, washed with water for three times, dried at 70 ºC overnight, recovered and reused without further treatment. As presented in Fig. 12, after the first use of photocatalyst 25% reduction in the efficiency was ocured, but the catalyst efficiency in the next runs remains constant at the same value. It can be concluded that the catalyst has a relatively acceptable reusability capacity.

Fig. 12.

3.4. photocatalytic degradation in real wastewater

To understand the practical application of developed photocatalyst for photocatalytic degradation of tetracycline in real wastewater more experiments were conducted using NST/CS nano-composite. In this regard experiments were carried out using a hospital's effluent (containing total dissolved solids of ~990 mg/l and chemical oxygen demand of ~225 mg/l). The wastewater was spiked with 10 mg/l of TC. Under optimized conditions the efficiency of photo-degradation of TC were lower in real wastewater than distilled water. The degradation efficiency of 76.6% was obtained in real wastewater compared to 91% degradation in distilled water. The composition of real wastewater including both organic and inorganic compounds leading to consumption of reactive species in side reactions which in turn affect the degradation efficiency.

4. Conclusion

The chitosan blended and unblended NST and NSZ photocatalysts were successfully synthesized and used for visible light degradation of TC. Among all, NST/CS showed the highest TC degradation. Different experimental techniques providing some structural details about synthesized NST/CS catalyst. The mix-crystal TiO_2 contains both anatase (82%) and rutile (18%) phases, thus exhibit higher photoactivity. The absorption tail of NST/CS is extended in the 400–800 nm region which increase the visible light absorption which consequently increases photocatalytic activity. RSM study was conducted and photocatalytic activity of the photocatalyst is mainly influenced by irradiation time and catalyst dose followed by pH and initial concentration of drug. The high photocatalytic performance of the NST/CS nano-composite is affected by some factors such as simultaneous participation of adsorption and photodegradation, narrowing of band gap and visible light promotion. This as-synthesized nano-composite has good reusability and also possesses high adaptability with different water conditions. NST/CS was found to be very active for visible light photocatalytic degradation of tetracycline from water/wastewater from pharmaceutical effluent.

Acknowledgements

The authors gratefully acknowledge the Research Council of Kermanshah University of Medical Sciences

(Grant Number: 96476) for the financial assistance.

References

Acosta, R., Fierro, V., Martinez de Yuso, A., Nabarlatz, D., Celzard, A., 2016. Tetracycline adsorption onto activated carbons produced by KOH activation of tyre pyrolysis char. Chemosphere 149, 168-176.
Ahmed, M.J., 2017. Adsorption of quinolone, tetracycline, and penicillin antibiotics from aqueous solution using activated carbons: Review. Environmental Toxicology and Pharmacology 50, 1-10.
Ani, I.J., Akpan, U.G., Olutoye, M.A., Hameed, B.H., 2018. Photocatalytic degradation of pollutants in petroleum refinery wastewater by TiO2- and ZnO-based photocatalysts: Recent development. Journal of Cleaner Production 205, 930-954.
Bahrami, H., Eslami, A., Nabizadeh, R., Mohseni-Bandpi, A., Asadi, A., Sillanpää, M., 2018. Degradation of trichloroethylene by sonophotolytic-activated persulfate processes: Optimization using response surface methodology. Journal of Cleaner Production 198, 1210-1218.
Bechambi, O., Sayadi, S., Najjar, W., 2015. Photocatalytic degradation of bisphenol A in the presence of C-doped ZnO: effect of operational parameters and photodegradation mechanism. Journal of Industrial and Engineering Chemistry 32, 201-210.
Bozorgpour, F., Ramandi, H.F., Jafari, P., Samadi, S., Yazd, S.S., Aliabadi, M., 2016. Removal of nitrate and phosphate using chitosan/Al 2 O 3/Fe 3 O 4 composite nanofibrous adsorbent: Comparison with chitosan/Al 2 O 3/Fe 3 O 4 beads. International journal of biological macromolecules 93, 557-565.
Buxton, G.V., Greenstock, C.L., Helman, W.P., Ross, A.B., 1988. Critical review of rate constants for reactions of hydrated electrons, hydrogen atoms and hydroxyl radicals (· OH/· O− in aqueous solution. Journal of physical and chemical reference data 17(2), 513-886.
Chang, P.-H., Li, Z., Yu, T.-L., Munkhbayer, S., Kuo, T.-H., Hung, Y.-C., Jean, J.-S., Lin, K.-H., 2009. Sorptive removal of tetracycline from water by palygorskite. Journal of Hazardous Materials 165(1), 148-155.
Cheng, X., Liu, H., Chen, Q., Li, J., Wang, P., 2013. Construction of N, S codoped TiO2 NCs decorated TiO2 nano-tube array photoelectrode and its enhanced visible light photocatalytic mechanism. Electrochimica Acta 103, 134-142.
Chiou, M.-S., Ho, P.-Y., Li, H.-Y., 2004. Adsorption of anionic dyes in acid solutions using chemically cross-linked chitosan beads. Dyes and pigments 60(1), 69-84.
D'Arienzo, M., Scotti, R., Wahba, L., Battocchio, C., Bemporad, E., Nale, A., Morazzoni, F., 2009. Hydrothermal N-doped TiO2: Explaining photocatalytic properties by electronic and magnetic identification of N active sites. Applied Catalysis B: Environmental 93(1), 149-155.
Dhanya, A., Aparna, K., 2016. Synthesis and Evaluation of TiO2/Chitosan Based Hydrogel for the Adsorptional Photocatalytic Degradation of Azo and Anthraquinone Dye under UV Light Irradiation. Procedia Technology 24, 611-618.
Eslami, A., Amini, M.M., Yazdanbakhsh, A.R., Mohseni-Bandpei, A., Safari, A.A., Asadi, A., 2016. N,S co-doped TiO2 nanoparticles and nanosheets in simulated solar light for photocatalytic degradation of non-steroidal anti-inflammatory drugs in water: a comparative study. Journal of Chemical Technology & Biotechnology 91(10), 2693-2704.
Gao, Y., Li, Y., Zhang, L., Huang, H., Hu, J., Shah, S.M., Su, X., 2012. Adsorption and removal of tetracycline antibiotics from aqueous solution by graphene oxide. Journal of colloid and interface science 368(1), 540-546.

Gregorio-Jauregui, K.M., Pineda, M.G., Rivera-Salinas, J.E., Hurtado, G., Saade, H., Martinez, J.L., Ilyina, A., López, R.G., 2012. One-step method for preparation of magnetic nanoparticles coated with chitosan. Journal of Nanomaterials 2012, 4.
Gu, L., Chen, Z., Sun, C., Wei, B., Yu, X., 2010. Photocatalytic degradation of 2, 4-dichlorophenol using granular activated carbon supported TiO2. Desalination 263(1-3), 107-112.
Hayon, E., Treinin, A., Wilf, J., 1972. Electronic spectra, photochemistry, and autoxidation mechanism of the sulfite-bisulfite-pyrosulfite systems. SO2-, SO3-, SO4-, and SO5-radicals. Journal of the American Chemical Society 94(1), 47-57.
Kakavandi, B., Takdastan, A., Jaafarzadeh, N., Azizi, M., Mirzaei, A., Azari, A., 2016. Application of Fe3O4@C catalyzing heterogeneous UV-Fenton system for tetracycline removal with a focus on optimization by a response surface method. Journal of Photochemistry and Photobiology A: Chemistry 314, 178-188.
Kamal, T., Anwar, Y., Khan, S.B., Chani, M.T.S., Asiri, A.M., 2016. Dye adsorption and bactericidal properties of TiO2/chitosan coating layer. Carbohydrate Polymers 148, 153-160.
Kannusamy, P., Sivalingam, T., 2013. Synthesis of porous chitosan–polyaniline/ZnO hybrid composite and application for removal of reactive orange 16 dye. Colloids and Surfaces B: Biointerfaces 108, 229-238.
Karthikeyan, K., Nithya, A., Jothivenkatachalam, K., 2017. Photocatalytic and antimicrobial activities of chitosan-TiO 2 nanocomposite. International Journal of Biological Macromolecules.
Karthikeyan, K.T., Nithya, A., Jothivenkatachalam, K., 2017. Photocatalytic and antimicrobial activities of chitosan-TiO2 nanocomposite. International Journal of Biological Macromolecules 104, 1762-1773.
Langford, J.I., Wilson, A.J.C., 1978. Scherrer after sixty years: A survey and some new results in the determination of crystallite size. Journal of Applied Crystallography 11(2), 102-113.
Martinez, C.R., Joshi, P., Vera, J.L., Ramirez-Vick, J.E., Perales, O., Singh, S.P., 2011. Cytotoxic studies of PEG functionalized ZnO Nanoparticles on MCF-7 cancer cells, NSTI Nanotechnology Conference and Expo, NSTI-Nanotech. pp. 420-423.
Nasseh, N., Taghavi, L., Barikbin, B., Nasseri, M.A., 2018. Synthesis and characterizations of a novel FeNi3/SiO2/CuS magnetic nanocomposite for photocatalytic degradation of tetracycline in simulated wastewater. Journal of Cleaner Production 179, 42-54.
Nasseri, S., Omidvar Borna, M., Esrafili, A., Rezaei Kalantary, R., Kakavandi, B., Sillanpää, M., Asadi, A., 2018. Photocatalytic degradation of malathion using Zn2+-doped TiO2 nanoparticles: statistical analysis and optimization of operating parameters. Applied Physics A 124(2), 175.
Nawi, M.A., Jawad, A.H., Sabar, S., Ngah, W.S.W., 2011. Immobilized bilayer TiO2/chitosan system for the removal of phenol under irradiation by a 45watt compact fluorescent lamp. Desalination 280(1), 288-296.
Nezamzadeh-Ejhieh, A., Karimi-Shamsabadi, M., 2013. Decolorization of a binary azo dyes mixture using CuO incorporated nanozeolite-X as a heterogeneous catalyst and solar irradiation. Chemical engineering journal 228, 631-641.
Norvill, Z.N., Toledo-Cervantes, A., Blanco, S., Shilton, A., Guieysse, B., Muñoz, R., 2017. Photodegradation and sorption govern tetracycline removal during wastewater treatment in algal ponds. Bioresource Technology 232, 35-43.
Pirsaheb, M., Asadi, A., Sillanpää, M., Farhadian, N., 2018. Application of carbon quantum dots to increase the activity of conventional photocatalysts: A systematic review. Journal of Molecular Liquids 271, 857-871.
Qiu, Y., Yang, M., Fan, H., Xu, Y., Shao, Y., Yang, X., Yang, S., 2013. Synthesis and characterization of nitrogen doped ZnO tetrapods and application in photocatalytic degradation of organic pollutants under visible light. Materials Letters 99, 105-107.
Rastkari, N., Eslami, A., Nasseri, S., Piroti, E., Asadi, A., 2017. Optimizing Parameters on Nanophotocatalytic Degradation of Ibuprofen Using UVC/ZnO Processes by Response Surface Methodology. Polish Journal of Environmental Studies 26(2), 785-794.
Salarian, A.-A., Hami, Z., Mirzaei, N., Mohseni, S.M., Asadi, A., Bahrami, H., Vosoughi, M., Alinejad, A., Zare, M.-R., 2016. N-doped TiO2 nanosheets for photocatalytic degradation and mineralization of

diazinon under simulated solar irradiation: Optimization and modeling using a response surface methodology. Journal of Molecular Liquids 220, 183-191.
Saravanan, R., Aviles, J., Gracia, F., Mosquera, E., Gupta, V.K., 2018. Crystallinity and lowering band gap induced visible light photocatalytic activity of TiO2/CS (Chitosan) nanocomposites. International Journal of Biological Macromolecules 109, 1239-1245.
Shao, G.-S., Zhang, X.-J., Yuan, Z.-Y., 2008. Preparation and photocatalytic activity of hierarchically mesoporous-macroporous TiO2−xNx. Applied Catalysis B: Environmental 82(3), 208-218.
Shao, L., Ren, Z., Zhang, G., Chen, L., 2012. Facile synthesis, characterization of a MnFe2O4/activated carbon magnetic composite and its effectiveness in tetracycline removal. Materials Chemistry and Physics 135(1), 16-24.
SİMSEK, E.B., 2017. Investigation of Photocatalytic Activity of Chitosan/Poly (vinyl alcohol)/TiO2/Boron Nanocomposites. Süleyman Demirel Üniversitesi Fen Bilimleri Enstitüsü Dergisi 21(2), 299-305.
Wu, F.-C., Tseng, R.-L., Juang, R.-S., 2001. Enhanced abilities of highly swollen chitosan beads for color removal and tyrosinase immobilization. Journal of Hazardous Materials 81(1-2), 167-177.
Xiang, Q., Yu, J., Jaroniec, M., 2011. Nitrogen and sulfur co-doped TiO2 nanosheets with exposed {001} facets: synthesis, characterization and visible-light photocatalytic activity. Physical Chemistry Chemical Physics 13(11), 4853-4861.
Yu, C., Cai, D., Yang, K., Yu, J.C., Zhou, Y., Fan, C., 2010. Sol–gel derived S,I-codoped mesoporous TiO2 photocatalyst with high visible-light photocatalytic activity. Journal of Physics and Chemistry of Solids 71(9), 1337-1343.
Zainal, Z., Hui, L.K., Hussein, M.Z., Abdullah, A.H., 2009. Characterization of TiO2–Chitosan/Glass photocatalyst for the removal of a monoazo dye via photodegradation–adsorption process. Journal of Hazardous Materials 164(1), 138-145.
Zhang, Y., Yan, W., Sun, Z., Pan, C., Mi, X., Zhao, G., Gao, J., 2015. Fabrication of porous zeolite/chitosan monoliths and their applications for drug release and metal ions adsorption. Carbohydrate Polymers 117, 657-665.
Zhu, H., Jiang, R., Fu, Y., Guan, Y., Yao, J., Xiao, L., Zeng, G., 2012. Effective photocatalytic decolorization of methyl orange utilizing TiO2/ZnO/chitosan nanocomposite films under simulated solar irradiation. Desalination 286, 41-48.

Table 1 Independent process variables and their levels in the experimental design

Variable	Symbol	Coded levels of variables

		-α	-1	0	1	+α
pH	A	5	6	7	8	9
Catalyst dose	B	0.5	1	1.5	2	2.5
Drug concentration	C	10	20	30	40	50
Time	D	20	30	40	50	60

Table 2 BET surface areas, pore volume, and pore size in the samples

sample	S_{BET} (m^2/g)[a]	Pore volume (cm^3/g)[b]	Average pore size (nm)[c]
NST	8.33	0.104	46.9
NSZ	17.80	0.360	63.2
NST/CS	0.49	0.011	84.1
NSZ/CS	2.09	0.022	89.0

[a]BET surface area calculated from the linear part of the BET plot. [b]BJH Adsorption cumulative volume of poresbetween 17.0 Å and 3 000.0 Å diameter. [c]Adsorption average pore diameter (4V/A by BET)

Table 3 A CCD matrix along with the observed process response.

Run No.	pH	Catalyst dose (g/l)	TC concentration (mg/l)	Time (min)	TC degradation (%)
1	8	2	40	50	87
2	7	1.5	30	40	54.28
3	7	1.5	50	40	54.83
4	8	2	40	30	83
5	6	1	20	30	68.75
6	8	1	40	50	86
7	5	1.5	30	40	63.5
8	8	2	20	50	74.41
9	7	1.5	30	40	58.2
10	8	2	20	30	45.83
11	7	2.5	30	40	74.28
12	7	1.5	30	40	59.9
13	8	1	40	30	79
14	7	1.5	30	40	63.1
15	6	2	40	30	64
16	7	1.5	30	40	56.6
17	6	2	20	30	87
18	6	2	40	50	86
19	6	2	20	50	89
20	9	1.5	30	40	79.48
21	6	1	40	30	39.58
22	7	0.5	30	40	58.51
23	7	1.5	30	40	52.3
24	6	1	20	50	81.25
25	8	1	20	50	77.08
26	6	1	40	50	56.25
27	7	1.5	10	40	76.95
28	7	1.5	30	60	75.71
29	8	1	20	30	68.75
30	7	1.5	30	20	46

Table 4 ANOVA results for the predicted quadratic model

Source	Sum of Squares	df	Mean Square	F-value	p-value
Model	4946.02	14	353.29	6.69	0.0004
A-pH	156.06	1	156.06	2.96	0.1061
B-Catalyst dose	345.95	1	345.95	6.55	0.0218
C-Drug concentration	128.25	1	128.25	2.43	0.1399
D-time	1073.34	1	1073.34	20.33	0.0004
AB	634.54	1	634.54	12.02	0.0035
AC	1389.43	1	1389.43	26.32	0.0001
AD	1.73	1	1.73	0.033	0.8588
BC	215.80	1	215.80	4.09	0.0614
BD	9.12	1	9.12	0.17	0.6836
CD	0.19	1	0.19	0.003	0.9531
A^2	609.72	1	609.72	11.55	0.0040
B^2	324.78	1	324.78	6.15	0.0255
C^2	301.38	1	301.38	5.71	0.0305
D^2	115.95	1	115.95	2.20	0.1591
Residual	791.92	15	52.79		
Lack of fit	716.16	10	71.62	4.73	0.0502
Pure error	75.76	5	15.15		
Cor Total	5737.95	29			
R^2: 0.8652, Adjusted R^2: 0.7332					

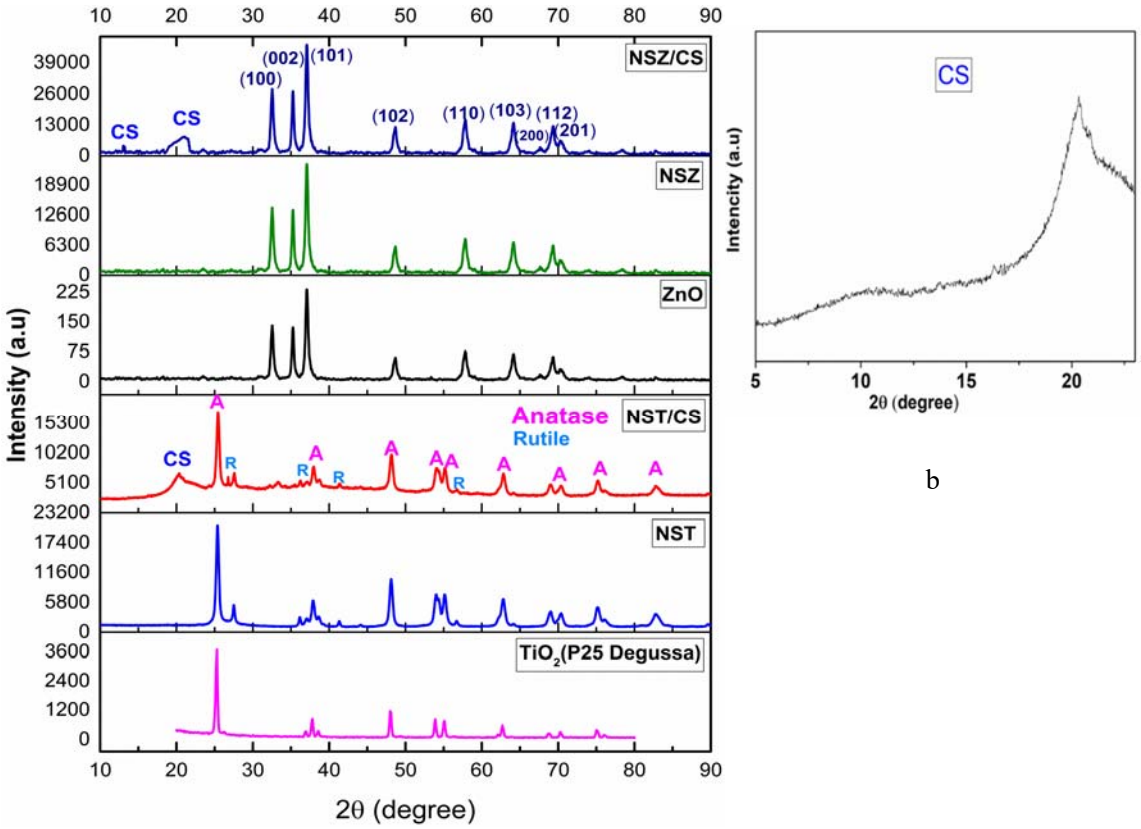

Fig. 1. XRD patterns of the TiO_2 Degussa P25, NST, NST/CS, ZnO, NSZ and NSZ/CS

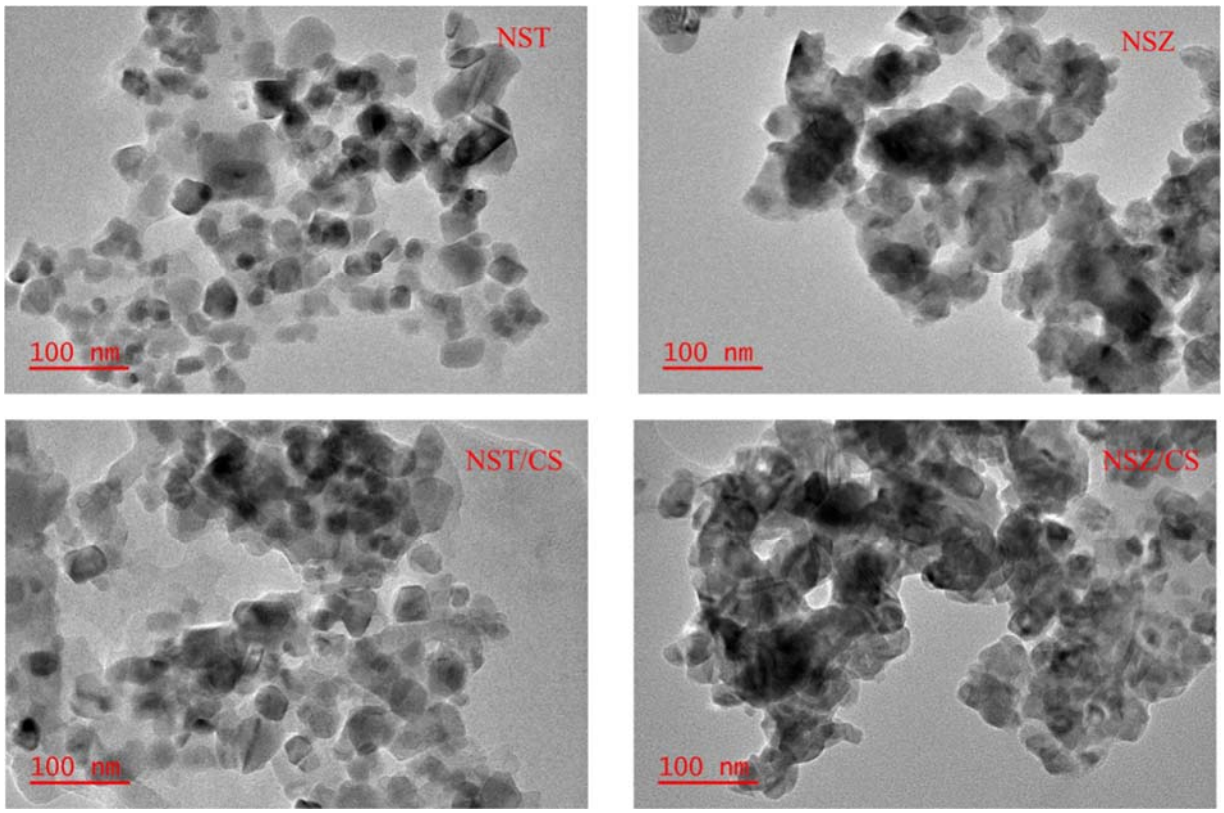
NST
100 nm
NSZ
100 nm
NST/CS
100 nm
NSZ/CS
100 nm

a

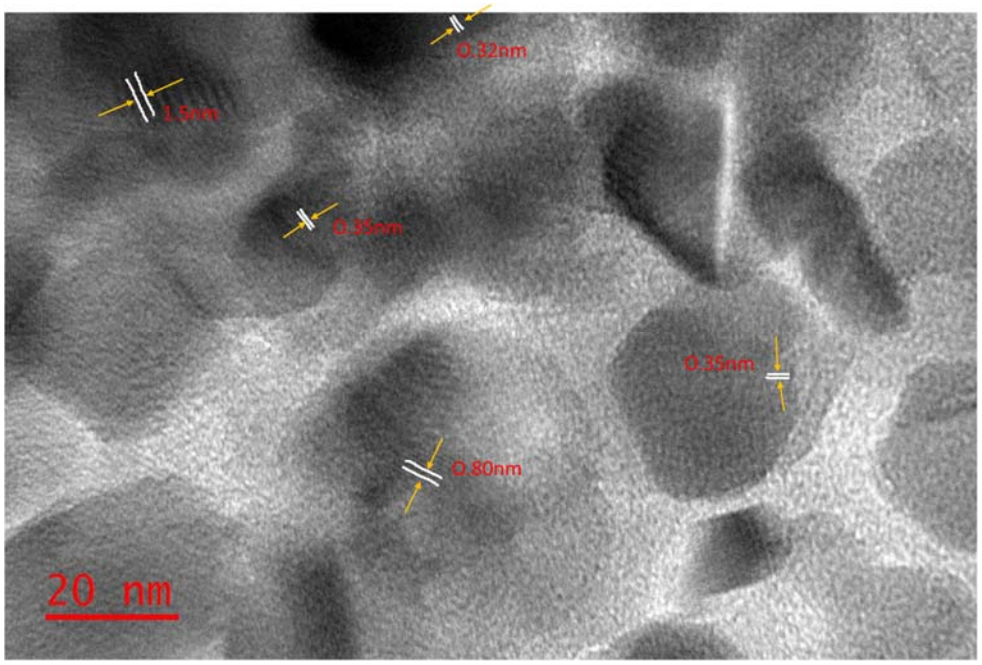
0.32nm
1.5nm
0.35nm
0.35nm
0.80nm
20 nm

b

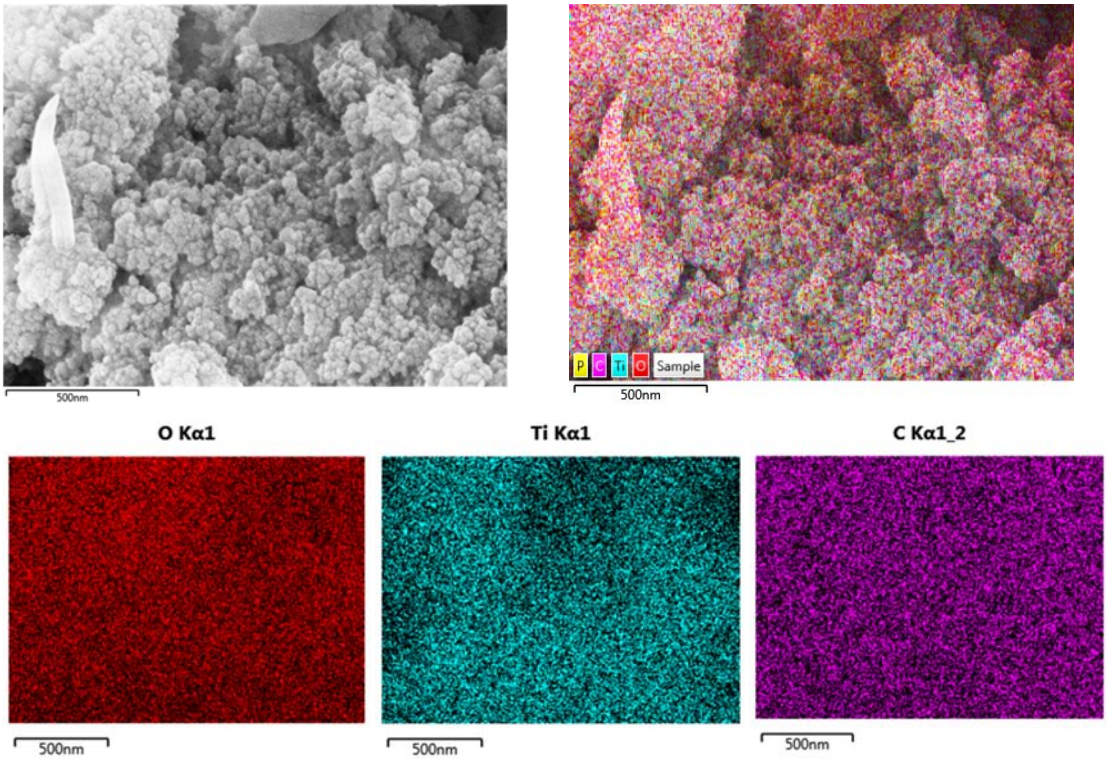

c

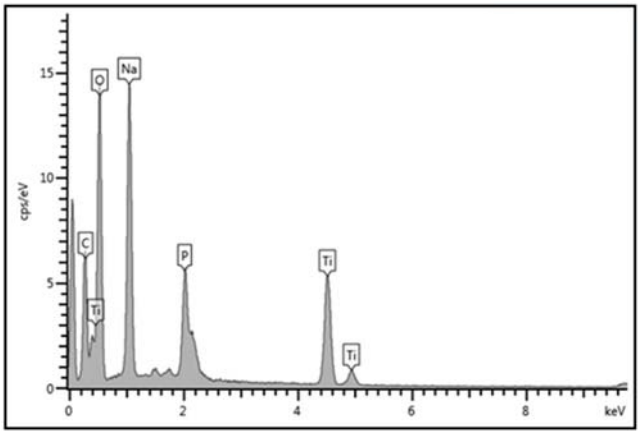

NST/CS	Wt%	Wt% Sigma
C	32.94	0.36
O	43.98	0.32
Na	13.25	0.13
P	2.85	0.05
Ti	6.97	0.08
Total	100.00	

d

Fig. 2. a) TEM images of samples NSZ, NST, NST/CS and NSZ/CS, b) HRTEM image of NST/CS nano-composite and c) SEM image of NST/CS with element distributions maps of O, Ti and C and d) Energy dispersive spectra (EDS)

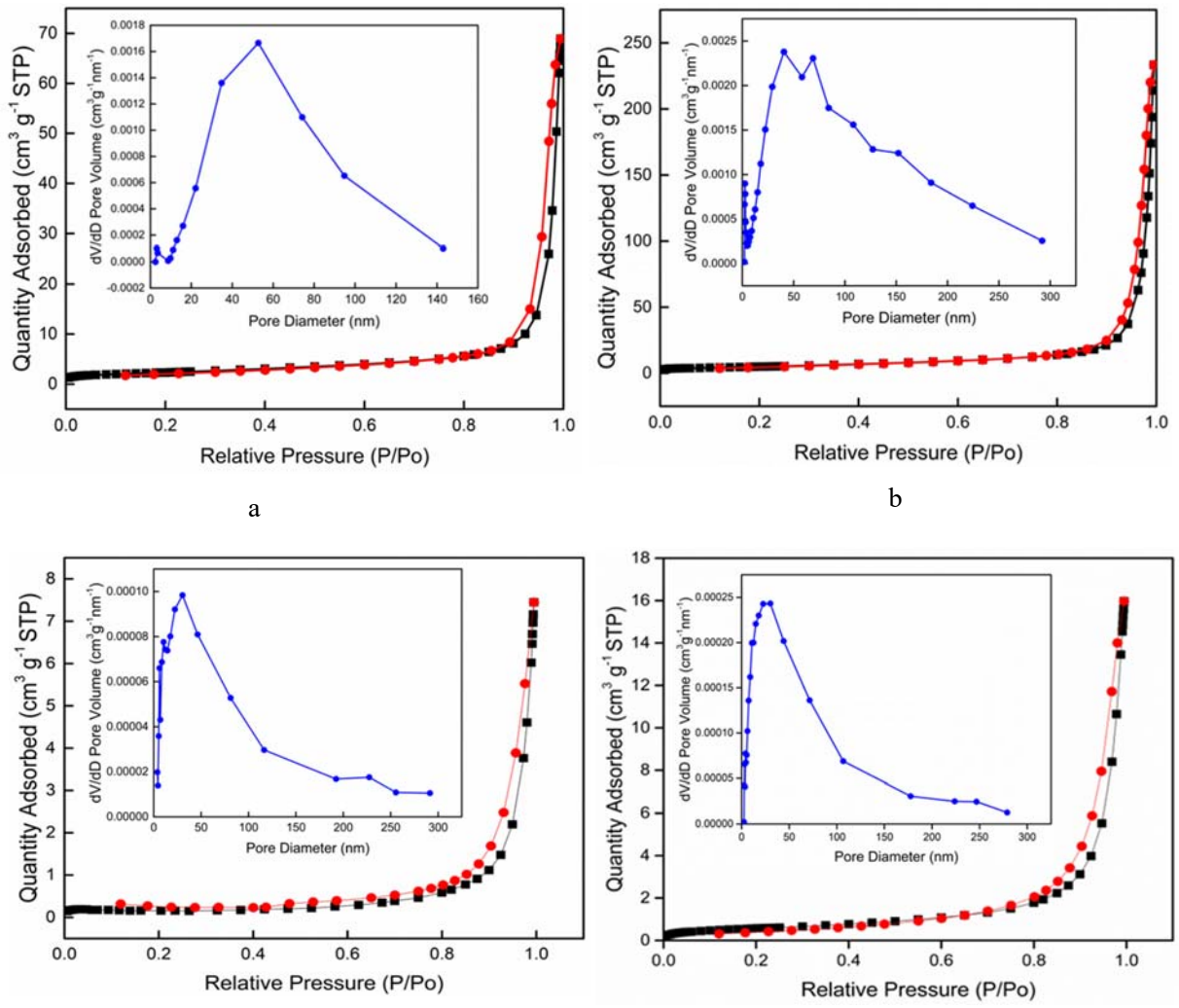

Fig. 3. N_2-sorption isotherms (adsorption —■—,desorption —●—) and corresponding pore-size distribution (inset) curves for the doped and blended samples: (a) NST, (b) NSZ, (c) NST/CS and (d) NSZ/CS

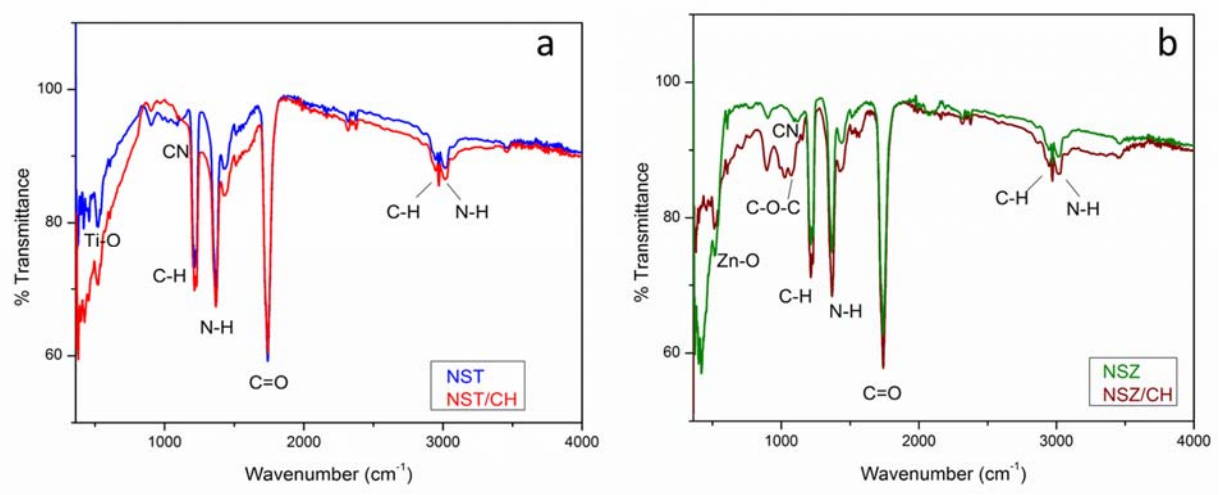

Fig. 4. FTIR spectra of (a) NST and NST/CS (b) NSZ, and NSZ/CS photocatalysts.

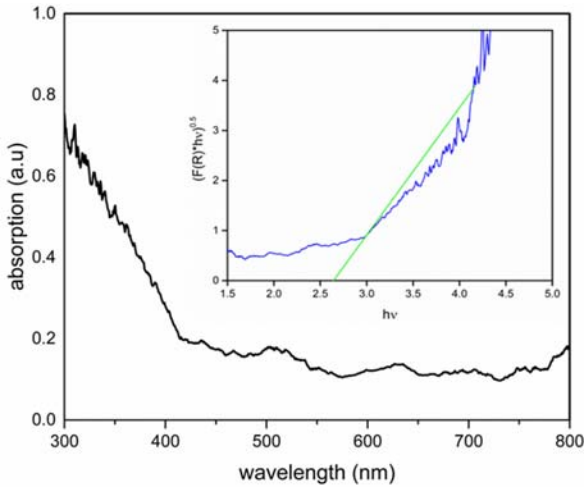

Fig. 5. UV-visible diffuse reflectance spectrum of NST/CS photocatalyst. Inset shows the corresponding Kubelka–Munk transformed reflectance spectrum.

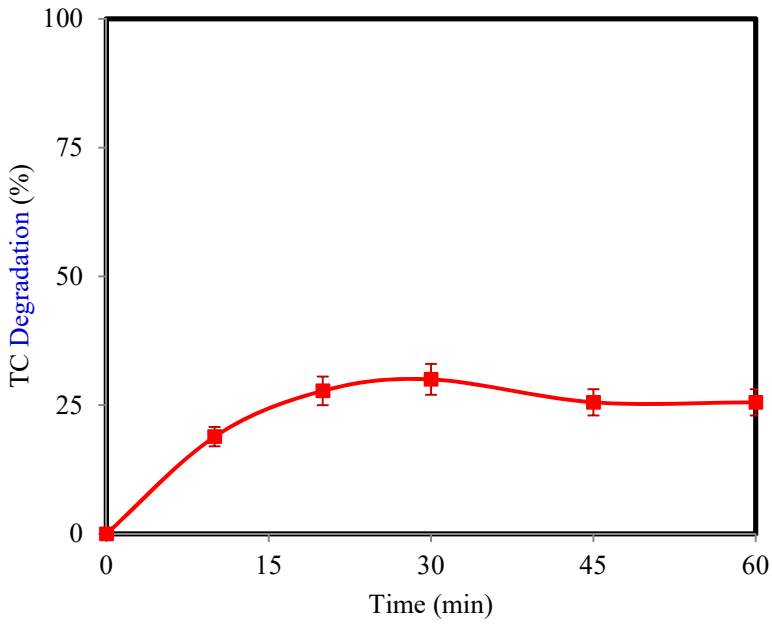

Fig. 6. Photolysis of TC (pH 7, initial TC concentration = 25.0 mg/l)

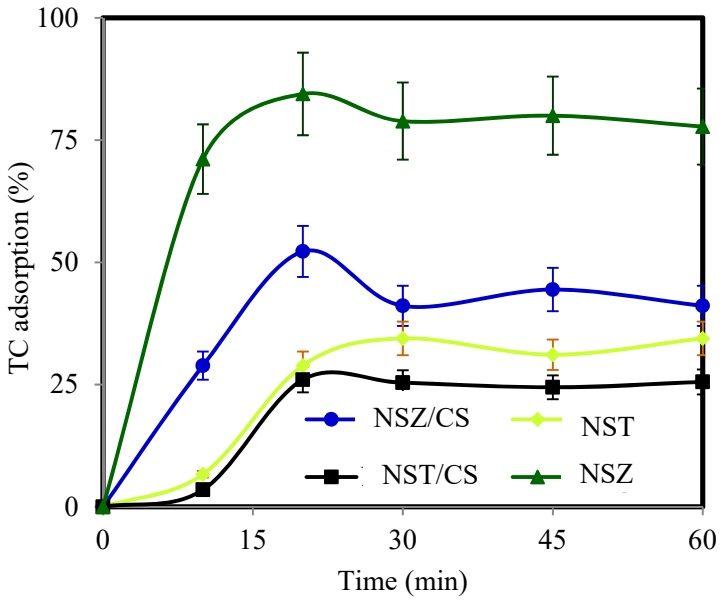

Fig. 7. Adsorption of TC on the different synthesized catalysts (initial TC concentration=25.0 mg/l, initial pH=7, catalyst dose=1.0 g/l).

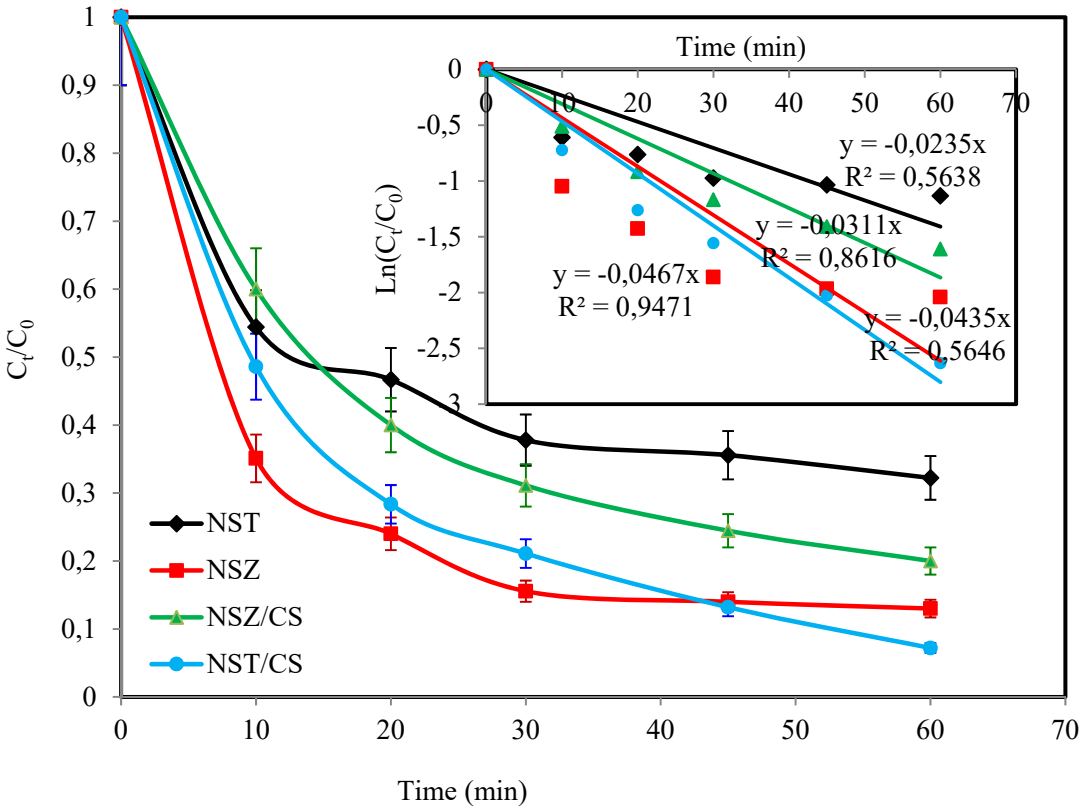

Fig. 8. Photocatalytic degradation of TC over different catalysts under visible light irradiation (pH 7, catalyst dose = 1.0 g/l, initial TC concentration = 25.0 mg/l). Inset shows the kinetic behavior of TC degradation over various photocatalysts.

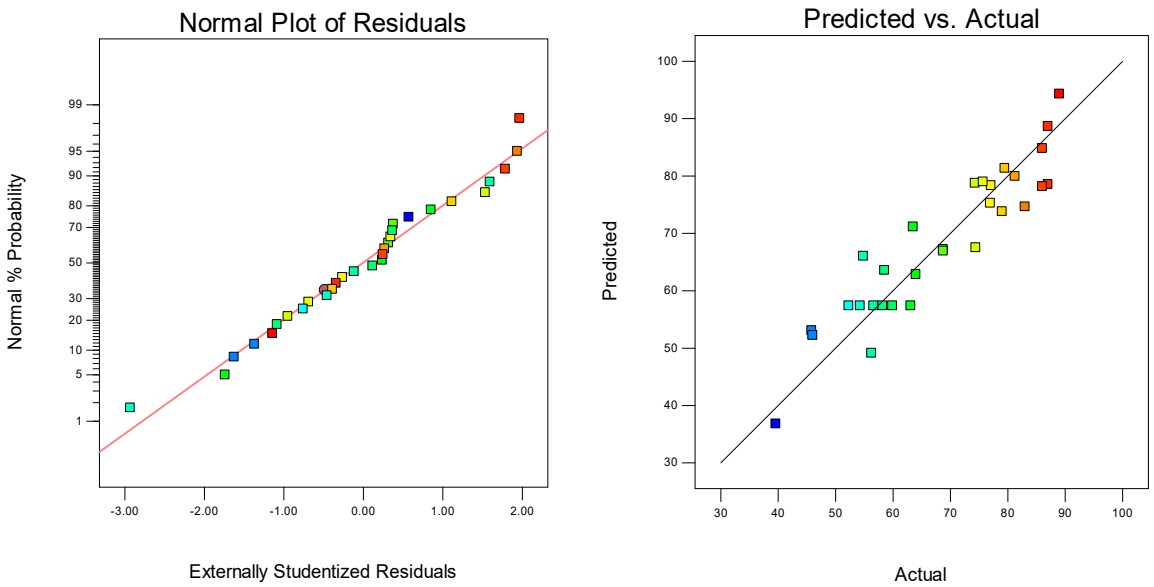

a b

Fig. 9. a) the normal probability plot of the residuals, and b) a plot of the predicted versus the actual photocatalytic degradation

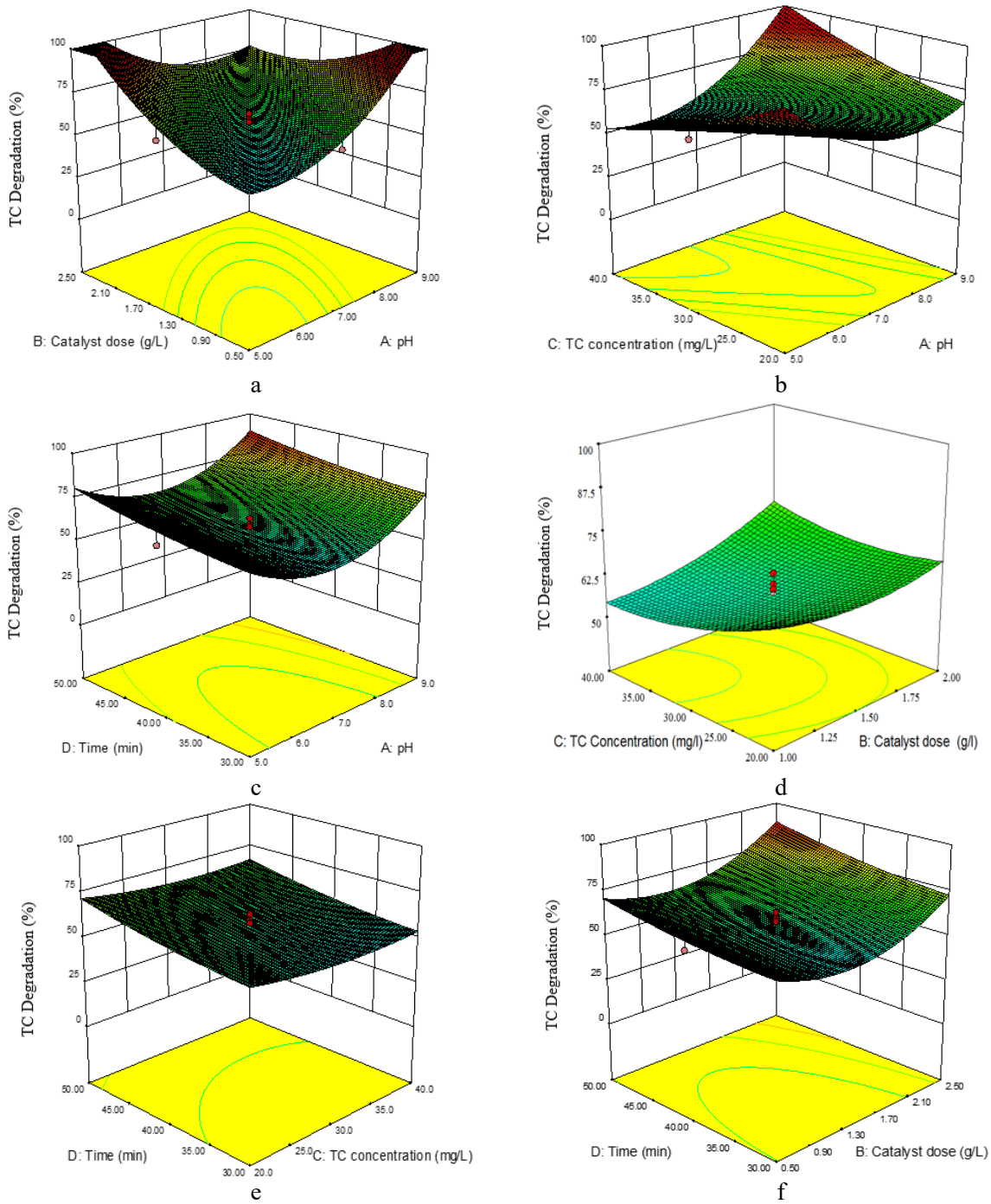

Fig. 10. 3D response surfaces for TC degradation using photocatalysis as a function of the process variables.

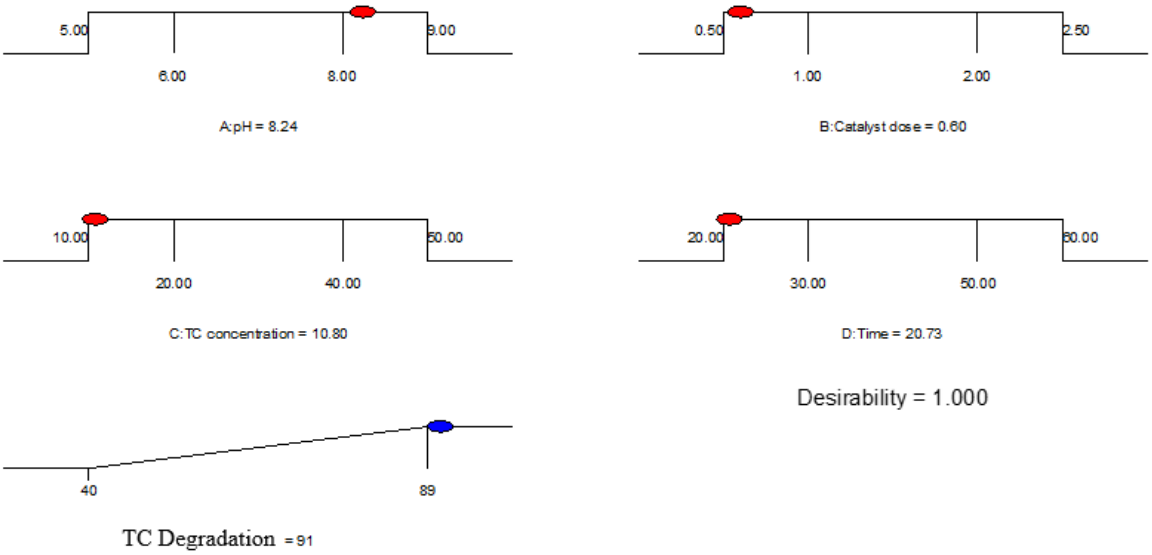

Fig. 11. Desirability ramp for numerical optimization of four goals solution pH, catalyst dose, TC concentration and contact time and degradation efficiency.

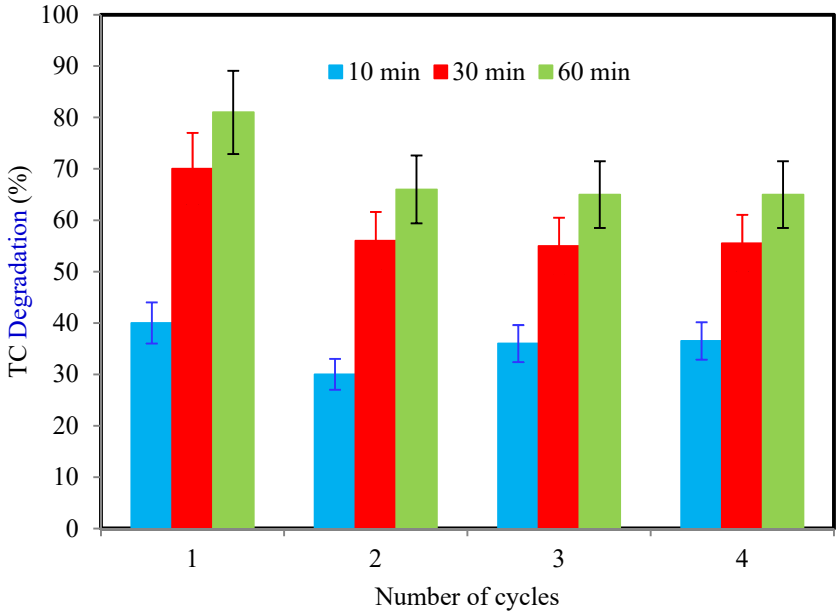

Fig. 12. Reusability of NST/CS nano-composite under optimum photocatalytic conditions